Measles virus co-opts epithelial-to-mesenchymal transition and live cell extrusion to exit human airway epithelia

Camilla E. Hippee[1], Lorellin A. Durnell[1], Justin W. Kaufman[2], Eileen Murray[2], Brajesh K. Singh[2], and Patrick L. Sinn[1,2†]

[1]Microbiology and Immunology, Carver College of Medicine, The University of Iowa, Iowa City, IA, 52242, USA

[2]Stead Family Department of Pediatrics, Carver College of Medicine, The University of Iowa, Iowa City, IA, 52242, USA

[†]Corresponding author: Patrick L. Sinn, Stead Family Department of Pediatrics, 169 Newton Rd, 6318 PBDB, The University of Iowa, Iowa City, IA, 52242, USA, Tel: (319) 335-8190, Fax: 319-335-9412, Email: patrick-sinn@uiowa.edu

Short title: Measles virus exits airway epithelia via cell detachment pathways

Key words: wound healing; cell detachment; viral infection; primary human cells; sphingosine kinase; TGF-β

Formatting for JVI

ABSTRACT

Measles virus (MeV) is a highly contagious respiratory virus transmitted via aerosols. To understand how MeV exits the airways of an infected host, we use unpassaged primary cultures of human airway epithelial cells (HAE). MeV typically remains cell-associated in HAE and forms foci of infection, termed infectious centers, by directly spreading cell-to-cell. We previously described the phenomenon in which infectious centers detach *en masse* from HAE and remain viable. Here we investigate the mechanism of this cellular detachment. Via immunostaining, we observed loss of tight junction and cell adhesion proteins within infectious centers. These morphological changes indicate activation of epithelial-to-mesenchymal transition (EMT). EMT can contribute to wound healing in respiratory epithelia by mobilizing nearby cells. Inhibiting TGF-β, and thus EMT, reduced infectious center detachment. Compared to uninfected cells, MeV-infected cells also expressed increased levels of sphingosine kinase 1 (SK1), a regulator of live cell extrusion. Live cell extrusion encourages cells to detach from respiratory epithelia by contracting the actomyosin of neighboring cells. Inhibition or induction of live cell extrusion impacted infectious center detachment rates. Thus, these two related pathways contributed to infectious center detachment in HAE. Detached infectious centers contained high titers of virus that may be protected from the environment, allowing the virus to live on surfaces longer and infect more hosts. This mechanism may contribute to the highly contagious nature of MeV.

IMPORTANCE

Measles virus (MeV) is an extremely contagious respiratory pathogen that continues to cause large, disruptive outbreaks each year. Here, we examine a phenomenon that may help explain the contagious nature of MeV: detachment of MeV-infected cells. MeV spreads cell-to-cell in human airway epithelial cells (HAE) to form groups of infected cells, termed “infectious centers”. We reported that infectious centers ultimately detach from HAE as a unit, carrying high titers of virus. Viral particles within cells may be more protected from environmental conditions, such as ultraviolet radiation and desiccation. We identified two host pathways, epithelial-to-mesenchymal transition and live cell extrusion, that contribute to infectious center detachment. Perturbing these pathways altered the kinetics of infectious centers detachment. These pathways influence one another and contribute to epithelial wound healing, suggesting infectious center detachment may be a usurped consequence of the host’s response to infection that benefits MeV by increasing its transmissibility between hosts.

INTRODUCTION

57 Measles virus (**MeV**) surpasses other respiratory viruses in transmissibility, but little evidence
58 exists to explain the contagious advantage of MeV. MeV is a morbillivirus in the paramyxovirus
59 family and, like other respiratory viruses, is primarily transmitted via aerosols. In an
60 unvaccinated population, an individual with RSV may spread virus to 3 others, while an
61 individual with MeV may spread virus to 12-18 others (1, 2). Vaccination rates must exceed 92%
62 for herd immunity; however, global vaccination rates have declined to 83% in the past two
63 years, leading to increased incidence of measles outbreaks and elevating MeV's status to an
64 imminent threat (3, 4, 5).
65
66 To model MeV respiratory infections, we use primary human airway epithelial cells (HAE). HAE
67 are derived from human lung donors and are directly seeded onto transwell filters without
68 passage (6). These cultures grow at an air-liquid interface, polarize, and differentiate into a
69 pseudostratified cell layer. HAE recapitulate the airways *in vivo* (7, 8). MeV infects HAE via its
70 epithelial cell receptor, nectin-4 (9, 10). Immune cells, such as dendritic cells or lymphocytes,
71 deliver the virus to nectin-4 on the basolateral side of HAE (11, 12). MeV then replicates in HAE
72 and spreads directly cell-to-cell via intercellular pores (13). MeV typically remains cell-
73 associated in HAE and forms foci of infection, termed infectious centers (shown schematically,
74 **Fig 1A**) (6, 13, 14). Infectious centers are unique to morbilliviruses; viruses outside of this genus
75 do not form infectious centers on HAE (13). Infectious centers are unique from syncytia and
76 multinucleated giant cells as the nuclei remain separate and the plasma membranes between
77 infected cells remain largely intact (6, 13). MeV infectious centers have been observed in HAE,
78 in human tracheal explants (6), and in the nasal passage, trachea, and bronchi of
79 experimentally infected macaques (15, 16).
80
81 Most respiratory viruses leave airway epithelial cells via apical budding, exocytosis, or cell lysis.
82 Many enveloped RNA respiratory viruses (e.g., IAV (17), RSV (18), and SARS-CoV-2 (19))
83 utilize apical budding at the host cell's plasma membrane to exit airway epithelial cells. Non-
84 enveloped viruses, like rhinovirus, exit via vesicles (exocytosis) or by bursting the cell open (cell
85 lysis) (20). MeV, an enveloped virus, was assumed to exit HAE via apical budding; however, we
86 found that MeV infection uniquely leads to dislodging of infectious centers containing
87 concentrated virus (**Fig 1A**) (21). Evidence for MeV-induced cell detachment is also found in
88 monkey epithelial cultures, *in vivo* monkey experiments, and human observation studies (15, 22,
89 23). The cellular signals that promote IC detachment are not known; however, cells of detached

infectious centers are metabolically active and do not display markers of cell death pathways, suggesting live cell extrusion pathways are involved (21, 23).

Here, we investigate the mechanism of infectious center detachment. As will be shown, single-cell RNA sequencing (21) suggests epithelial-to-mesenchymal transition (EMT) is activated within infectious centers. Airway epithelial cells are typically quiescent and nonmigratory. However, certain circumstances necessitate epithelial cells to divide and migrate. EMT is initiated by diverse stimuli to dissolve cell-cell connections and promote mobilization. EMT is involved in wound repair, tumor metastasis, and response to viral infection (24, 25, 26). Importantly, EMT encompasses a spectrum of intermediate cell types.

EMT signaling associates with live cell extrusion (LCE), a pathway driven by sphingosine kinase 1 (SK1). SK1 phosphorylates sphingolipids, which are cell signaling molecules that localize to membranes. In infected cells, increased SK1 activity drives pro-survival signaling that results in more virus production (27, 28, 29, 30, 31, 32). In addition, downstream signaling of SK1 directs neighboring cells to contract their actomyosin, creating a luminal force on the cell to be extruded (33, 34). Cell extrusion is important for maintaining homeostasis within epithelia and can be activated by several stimuli, including EMT, apoptosis, overcrowding, or loss of cell polarity (35, 36, 37). LCE and EMT signaling pathways overlap and each can activate the other. Here, we show that both pathways are active within infectious centers and contribute to detachment.

RESULTS

Single cell RNA-sequencing implicates two detachment pathways.

To investigate what pathways may be responsible for infectious center detachment, we probed our previously published single-cell RNA sequencing (scRNA-seq) dataset (21). In this dataset, HAE from 10 human donors were mock-infected or infected with a MeV expressing a GFP reporter protein (MeV-GFP). At multiple timepoints post-infection, samples were sorted via fluorescence-activated cell sorting (FACS) to enrich the GFP+ population before performing scRNA-seq. Lists of genes differentially expressed between mock and MeV infected (both GFP+ and GFP-) HAE were analyzed by gene ontology (**Fig 1B**). Many gene ontology terms from this analysis pointed to EMT processes, including “positive regulation of EMT”. Enrichment of gene products such as TGFB1, SNAI2, and metalloproteinases (MMPs) are emblematic of EMT (**Fig 1C**).

124 EMT-related mRNAs were notably increased in a distinct cluster of cells, termed “ISG-high” (**Fig**
125 **1D and 1E**). This cluster was exclusively observed in MeV-infected HAE cultures (**S1A Fig**),
126 contained ~80% GFP+ and ~20% GFP- cells, and the cells expressed unique transcriptomes
127 that did not align with known HAE cell types (**Fig 1D**). Previously, we erroneously dubbed these
128 cells as “interferon-high cells” due to elevated interferon-stimulated gene (ISG) transcripts (21).
129 However, further analysis revealed that expression of these ISGs was not interferon-mediated
130 (38). As such, we renamed these cells “ISG-high cells” and continue to investigate their
131 characteristics. We could not identify what cell type the ISG-high cells were before they were
132 infected possibly because of the transcriptional impact of EMT.
133
134 Notably, ISG-high cells had elevated SNAI2 transcripts, a transcriptional regulator of EMT (**Fig**
135 **1E and S1B Fig**). Further investigation of the transcriptional profiles of ISG-high cells revealed
136 a potential second detachment pathway: live cell extrusion (LCE). LCE is induced by
137 sphingosine kinase 1 (SK1), one of the top enriched gene products within the ISG-high cluster
138 (**Fig 1F and S1C Fig**). In this manuscript, we will separately consider EMT and LCE for
139 infectious center detachment.
140
141 *EMT is activated within infectious centers.*
142 We evaluated the role of EMT in MeV infection. Quantitative Real-Time PCR (qRT-PCR)
143 confirmed EMT-related gene transcripts are elevated in MeV-infected cultures (**S2A Fig**). In
144 addition, TGF-β, a potent inducer of EMT, was secreted in higher concentrations following MeV-
145 infection (**S2B Fig**). EMT is characterized by a loss of epithelial cell markers (39, 40, 41, 42).
146 Indeed, immunostaining of infectious centers at 3 days post-infection and 7 days post-infection
147 with MeV-mCherry showed a loss of β-catenin (**Fig 2A**), ZO-1 (**Fig 2B**), and E-Cadherin (**Fig**
148 **2C**). In all cases, the loss of the markers was more pronounced toward the center of the
149 infectious center. Degradation increased over time and ~60% of the infectious center area had
150 loss of the indicated junctional protein by day 7 (**Fig 2D**). Additionally, cells of infectious centers
151 may have altered apical-basal polarity, as evidenced by an atypical pattern of expression of the
152 apically targeted ezrin protein (arrow; **S2C Fig**). These results demonstrate EMT activation in
153 MeV-infected HAE.
154
155 *EMT contributes to infectious center detachment.*
156 Infectious center detachment can be tracked using live cell fluorescence microscopy. Images
157 were collected daily post-infection and the timepoint at which each infectious center detached

158 was documented (**Fig 3A**). These data were used to calculate a probability of detachment. To
159 determine the impact of EMT on infectious center detachment, we treated MeV-infected HAE
160 with a TGF-β inhibitor, SB431542, which blocks downstream transcriptional activation of TGF-β
161 (43, 44). With TGF-β inhibited, infectious centers detached at a slower rate than vehicle-treated
162 controls (**Fig 3B**). Titers (**Fig 3C**), infectious center number (**Fig 3D**), infectious center area (**Fig**
163 **3E**), and cytotoxicity (**Fig 3F**) were not statistically different between the treatment and control
164 groups, suggesting that TGF-β inhibition slows IC detachment without impacting viral replication
165 or cell-to-cell spread.
166
167 *LCE is activated within infectious centers.*
168 EMT can lead to LCE. Once a cell is fated for extrusion, sphingosine, a cellular lipid, is
169 phosphorylated by sphingosine kinase 1 (SK1) to produce sphingosine-1-phosphate (S1P) (**Fig**
170 **4A**). S1P binds its receptor, S1PR2, on neighboring cells, signaling for the activation of the Rho
171 pathway. As a result, a ring of cells surrounding the fated cell will contract their actomyosin,
172 creating an apical force to expel the cell (33, 34, 35, 37). Transcripts for *SK1*, Rho pathway
173 genes (*RHOA*, *RHOB*, and *RHOD*), and genes responsible for actomyosin contraction (*MYH9*
174 and *ROCK1*) (37, 45) were elevated within the ISG-high cell cluster of our scRNA-seq dataset
175 (**Fig 4B**). Immunostaining revealed altered SK1 localization within the cells of infectious centers
176 (**Fig 4C and 4D**). Specifically, SK1 was most abundant at the nucleus (arrows; **Fig 4D**).
177 Together, these data suggest SK1 is expressed in MeV-infected cells and initiates LCE
178 signaling.
179
180 *LCE contributes to infectious center detachment.*
181 Using the infectious center detachment assay described in Figure 3, we evaluated the impact of
182 an SK1 inhibitor on infectious center detachment. Treatment with the SK1 inhibitor, SKI-II,
183 delayed infectious center detachment (**Fig 5A**). SKI-II treatment did not cause a statistically
184 significant change in titers (**Fig 5B**), infectious center number (**Fig S3A**), or infectious center
185 area (**Fig S3B**) of MeV-infected HAE. To exacerbate LCE, MeV-infected HAE were treated with
186 exogenous S1P. The probability of infectious center detachment increased and infectious
187 centers detached faster (**Fig 5C**), despite viral titers (**Fig 5D**), infectious center number (**Fig**
188 **S3C**), infectious center area (**Fig S3D**), and cytotoxicity (**Fig S3E**) remaining statistically
189 indistinguishable to vehicle-treated controls. These results demonstrate infectious center
190 detachment utilizes LCE pathways.
191

192 DISCUSSION

193 Here, we showed that two overlapping, wound healing pathways are active within the cells of
194 infectious centers. Transcriptional regulators of EMT and LCE are elevated in MeV-infected
195 cells. Physical evidence of EMT and LCE was observed via immunostaining and microscopy.
196 Additionally, because infectious center detachment could be delayed by inhibiting EMT and LCE
197 and increased using an LCE agonist, we concluded that both pathways contribute to infectious
198 center detachment. Although not shown, we induced EMT in HAE with exogenous TGF-β
199 followed by MeV infection to determine if infectious center detachment increased. However, the
200 results were uninterpretable because infection of epithelial cells primed for EMT results in
201 widespread syncytial-like, multi-nucleated giant cells instead of discreet infectious centers. As
202 we previously reported, infectious center formation requires proper epithelial differentiation (6).
203 As primary epithelial cell culture has become more accessible, cell detachment has been
204 observed in several virus infections of epithelia. This includes astrovirus (46), rotavirus (47), and
205 enterovirus A71 (48). Both EMT and LCE are candidate mechanisms for cell detachment in
206 these infections and are potentially a common result of epithelial cell viral infection.
207
208 EMT and LCE pathways have important roles in maintaining homeostasis of the epithelial layer
209 and their functions often overlap (35, 45, 49, 50). LCE activates in cases of cell overcrowding
210 (34, 36, 51), removing damaged cells following injury (51), or following apoptotic signaling (37,
211 52, 53, 54). EMT is a key tool for wound healing and is active in chronic lung diseases like
212 idiopathic pulmonary fibrosis (55). In EMT, cells can gain actomyosin contractility, a key
213 mechanism for LCE (41). Transcriptional regulators of EMT, like SNAI1, impact RhoA signaling
214 and actomyosin contractility (45). Wee et al. (45) showed that cell-cell adhesion loss works
215 cooperatively with actomyosin contraction to cause cell extrusion. In a complementary manner,
216 SK1 promotes EMT by degrading cell-cell adhesions, like E-cadherin, and activating the focal
217 adhesion kinase pathway, which includes MMPs (56, 57). Inhibiting SK1 blocks signaling of two
218 EMT activators, NF-κB and TGF-β, whereas exogenous S1P treatment induces EMT (58, 59).
219 Notably, SK1 and SNAI2 coexpress within human tumors (60). In fact, LCE and EMT appear to
220 be so intertwined that one does not exist without the other. We postulate that, in the context of
221 MeV infection of HAE, EMT and LCE activate simultaneously and cooperate to expel infectious
222 centers. EMT likely promotes infectious center detachment by altering cell-cell adhesions, while
223 LCE mechanically promotes detachment via actomyosin contraction.
224

225 SK1 is involved in several viral infections because of its role in activating cell pro-survival
226 signaling (29, 30, 61, 62, 63, 64). A stressed cell will accumulate sphingosine in its plasma
227 membrane, marking the cell for apoptosis; however, in the presence of increased SK1
228 expression, sphingosine is phosphorylated by SK1 to create S1P, a signal for cell survival (37,
229 65, 66, 67). S1P prolongs the life of an infected cell and increases viral replication as the virus
230 has more time to propagate. Viral replication is associated with SK1 expression during infection
231 with respiratory syncytial virus (32), human cytomegalovirus (68), and influenza virus (28). In
232 cases of viral infections, SK1 expression is induced via TNF-α signaling and regulated by the
233 ERK/AKT pathway (69, 70, 71). MeV may also take advantage of SK1's cell survival phenotype
234 to increase virion production. Indeed, several genes of the TNF-α pathway were upregulated in
235 our scRNA-seq ISG-high cells (**Fig 4B**).
236
237 We observed SK1 expression in the nucleus of infected cells (**Fig 4C and 4D**). While SK1 is
238 more commonly found in the cytoplasm, nuclear localization is seen in human lungs with
239 idiopathic pulmonary fibrosis (72) and SK1 translocation to the nucleus is induced with estrogen
240 treatment of breast cancer cells (73). While the role of nuclear SK1 is still unclear, sphingosine
241 kinase 2 is known to alter gene expression in the nucleus and may render cells more resistant
242 to apoptosis (74). In addition, MeV replication was previously shown to be sensitive to SK1
243 inhibition in HEK 293 cells (30). In that study, NF-κB expression was necessary for MeV
244 replication and inhibiting SK1 equally inhibited NF-κB. In contrast, we did not find that SKI-II
245 treatment affected viral titers in HAE. This may be due to differences in cell types used since
246 HAE are much more resilient than HEK 293 cells to viral infections and are more likely to
247 survive. Importantly, immortalized tumor cells are likely to be inherently skewed toward a
248 mesenchymal phenotype even if they were originally derived from an epithelial cell. Thus,
249 unpassaged, primary epithelial cells may be better suited for studying viral induced EMT and
250 LCE.
251
252 EMT might also explain why infectious centers stop growing. Our recent work determined that
253 cell-cell spread of MeV is not restricted by interferon-induced innate immune signaling (38).
254 EMT causes the disassociation of cell-cell junctions, including adherens junctions (24). The MeV
255 receptor nectin-4 is localized in adherens junctions and is required for cell-cell spread (13). The
256 loss of adhesion caused by EMT could contribute to halted infectious center growth. This
257 sequestration of infectious centers from the rest of the epithelia may also explain why the cells
258 of infectious centers maintain their connections to one another while simultaneously losing their

connection to neighboring cells. While we do not have an answer for why cells of infectious centers remain attached to one another after they are dislodged, we have two hypotheses: 1) Cells with similar actin densities group together (75): as MeV infection degrades actin within infectious centers, the surface tension of the cellular membranes of infectious center cells may decrease, distinguishing these cells from the uninfected cells around them. 2) While mesenchymal-like cells do not integrate well within tissues during migration, they can form transient cell-cell adhesions with each other and nearby stationary cells (76). One such connection could be formed during the transfer of MeV factors through intercellular pores that form during cell-cell spread. Future studies identifying cell-cell adhesions that persist in MeV-infected cells will be key in determining the bottlenecks that impact infectious center growth and detachment.

We identified a group of “ISG-high cells” in our scRNA-seq that had high transcripts of ISGs as well as EMT and LCE markers. We postulate that these cells are either within infectious centers or are uninfected cells near the periphery of infectious centers (**Fig S1A**). These cells are responding to the infection, seemingly by increasing antiviral gene transcripts. In a recent publication, we studied interferon stimulation in HAE in the context of MeV infection and determined interferons are not produced at detectable levels (38). While the mystery of what initiates ISG transcription remains, we believe the name “ISG-high cells” more accurately describes this cluster than the previously reported “interferon high cells”(21). Importantly, we are not suggesting that ISG-high cells are a new epithelial cell type, but cells with an altered transcriptional profile following MeV infection. ISG-high cells were likely secretory or ciliated cells before MeV infection, but we cannot be sure because those cell type markers are not detectable in our samples. Understanding the influences that push cells towards the ISG-high cell transcriptome profile is of interest.

In summary, our results describe two, related pathways by which MeV extrudes groups of virus-laden cells. Infectious center detachment was altered by inhibitors and agonists of EMT and LCE, which supports our conclusion that MeV exits HAE via this strategy. Damage to the cell during MeV infection likely initiates these pathways and infectious center detachment is an unintended consequence that gives MeV an advantage. While vaccination remains the best preventative measure for MeV, understanding MeV infectious center detachment is vital for investigating the contagious nature of MeV and may prove helpful in healthcare settings.

293 MATERIALS AND METHODS

294 **Ethical statement.** The University of Iowa *In Vitro* Models and Cell Culture Core prepared the
295 well-differentiated primary cultures of human airway epithelia (HAE) used in these studies.
296 These cultures are comprised of cells from autopsy, discarded tissue, or surgical specimens. All
297 human subject studies were conducted with approval from the University of Iowa Institutional
298 Review Board. We do not receive identifiable information.

299

300 **Human airway epithelial cells.** HAE were cultured and maintained as previously described (6,
301 7). Briefly, cells from trachea and bronchus epithelia are seeded onto collagen-coated,
302 polycarbonate transwell inserts (0.4 μm pore size, surface area = 0.33 cm^2; Corning Costar;
303 #3413) following enzymatic disassociation. Cells were submerged in Ultroser G (USG) medium
304 at 37°C and 5% CO_2. After 48 hours, apical USG was removed and cells were incubated at the
305 air-liquid interface and allowed to polarize and differentiate. All HAE cultures used for the
306 experiments in this study were >3 weeks old and maintained a transepithelial electrical
307 resistance of at least 500 $\Omega \cdot \mu m^2$.

308

309 **Bioinformatic analyses.** The scRNA-seq dataset was previously described (21) and can be
310 accessed in the GEO with accession number GSE168775. In brief, MeV-infected or mock-
311 infected HAE (pooled from 10 human donors) were dissociated using TrypLE and sorted by
312 fluorescence-activated cell sorting to separate GFP- and GFP+ cells for scRNA-seq. ~30,000
313 cells make up the dataset. Gene ontology analysis was performed using GOrilla (77, 78). Violin
314 plots, t-SNE plots, and heatmap data were generated in Loupe Browser version 6.4.1.
315 Heatmaps were visualized with the R package gplots version 3.1.3.

316

317 **Measles virus production.** Recombinant MeV-GFP and MeV-mCherry viruses are derived
318 from the IC323 strain and were produced as previously described (79). Briefly, Vero cells that
319 stably express human SLAMF1 (80) were maintained in Dulbecco modified Eagle medium
320 (DMEM; Thermo Fisher Scientific) supplemented with 5% newborn calf serum (NCS; Thermo
321 Fisher Scientific) and penicillin-streptomycin (100 mg/mL; Thermo Fisher Scientific). Vero-
322 hSLAM cells were infected with either MeV-GFP for MeV-mCherry at an MOI of 0.01 for 2 hours.
323 2 days post-infection, cells were collected and subjected to several freeze/thaw cycles to induce
324 cell membrane rupture and virus release. Virus was titrated using $TCID_{50}$ assays with Vero-
325 hSLAMF1 cells. We have not detected differences in MeV-GFP and MeV-mCherry infections.

326 We selected MeV-GFP or MeV-mCherry for our experiments due to their compatibility with
327 reagents and instrumentation.
328
329 **Infection of HAE.** HAE cultures in this study were infected with MeV as previously published
330 (13, 14). Briefly, HAE cultures were inverted to expose the basolateral surface. 50 μL virus
331 inoculum, containing MeV virus and serum-free opti-MEM (Thermo Fisher Scientific;
332 #31985062) was placed on the basolateral side of the cells. Virus inoculum was incubated on
333 HAE for ~4 hours at 37°C and 5% CO_2. After the infection period, the inoculum was removed
334 and the cultures were placed back into an upright position with medium in the basolateral
335 chamber.
336
337 **Immunostaining and confocal microscopy.** All cells prepped for immunofluorescence were
338 fixed with 2% paraformaldehyde for 15 minutes followed by washing with 1X PBS and
339 permeabilization with 0.2% Triton X-100 in Superblock (Thermo Fisher Scientific; #37580) for 1
340 hour. All primary antibodies were used at 1:100 dilution in Superblock overnight at 4°C. After
341 overnight incubation, cells were washed 3x with 1X PBS and incubated with fluorescently
342 labelled secondary antibodies at a 1:1000 dilution in Superblock buffer for 1 hour at RT, gentle
343 rocking. HAE filters were cut from the transwell using a razor blade and mounted onto glass
344 microscope slides, covered with VECTASHIELD Mounting Medium with DAPI (Vector
345 Laboratories; #H-1200-10) and a glass coverslip overtop. Coverslips were sealed with clear nail
346 polish. For confocal analysis, a Leica SP8 STED confocal microscope (Leica Microsystems)
347 was used. Image processing was performed using ImageJ2 version 2.3.0. Primary antibodies
348 used: Beta-catenin (Thermo Fisher Scientific; #13-8400), ZO-1 (Thermo Fisher Scientific; #33-
349 9100), E-cadherin (Cell Signaling Technology; #3195), Ezrin (Cell Signaling Technology; #3145),
350 SK1 (Invitrogen; #PA5-28584). Secondary antibodies used: Goat Anti-Rabbit IgG Highly Cross-
351 Adsorbed (H+L) Alexa Fluor 568 (Invitrogen; #A-11036), Goat Anti-Mouse IgG Highly Cross-
352 Adsorbed (H+L) Alexa Fluor 546 (Invitrogen; #A-11030).
353
354 **Quantification of cytoskeleton breakdown**. Confocal images of 3, randomly selected
355 infectious centers were collected from 3 human donors for BCAT, ZO-1, and ECAD. Infectious
356 center area was measured using the freehand tool in ImageJ2 version 2.3.0. Adhesion
357 disruption area was determined by accumulating the area measurements of all protein
358 degradation within the infectious center. The data are plotted as a percentage: (total area of
359 degradation) / (total area of infectious center) x 100.

360

361 **Quantitative reverse transcriptase polymerase chain reaction (qRT-PCR**). At 3 dpi, mock-
362 and MeV-infected cell lysates were collected with TRIzol reagent (Thermo Fisher Scientific;
363 #15596026). Cellular RNA was isolated using the Direct-zol RNA Miniprep kit (Zymo Research;
364 #R2052). After isolation, RNA was transcribed into cDNA with the High-Capacity RNA-to-cDNA
365 kit and the manufacturer's instructions (Thermo Fisher Scientific; #R2052). qPCR of *MMP1*,
366 *MMP10*, *TGFB1*, *SNAI2*, and *SMAD3* was accomplished using primers, *Power*SYBR Green
367 Real-Time PCR Master Mix (Thermo Fisher Scientific; #4367659), and a QuantStudio 7 Pro
368 (Applied Biosystems). The housekeeping gene used was *SFRS9*. Primer sequences can be
369 found in Table S1.

370

371 **TGF-β ELISA.** Apical washes (100 µl Opti-MEM) and basolateral media (100 µl USG medium)
372 were collected from mock- and MeV-infected HAE. Secretions were measured in duplicate for
373 TGF-β protein content using a Human TGF-beta 1 ELISA Kit (RayBiotech; #ELH-TGFb1-1) and
374 following the manufacturer's protocol. ELISAs were read on XXX.

375

376 **Drug treatments.** SKI-II (MedChemExpress; #312636-16-1) and SB431542 (Tocris; #1614)
377 were diluted to 20 µM with USG medium. Recombinant S1P (Tocris; #1370) was diluted to 10
378 µM with USG medium. Treatments were placed in the basolateral chamber of the HAE cultures.
379 Equivalent volume of DMSO (4 µl) was diluted in USG medium for vehicle control cultures. SKI-
380 II and S1P treatments began 1-day post-infection. SB431542 treatment began 1 day pre-
381 infection. Treatments remained on the cells for the length of the experiment and
382 media/treatments were refreshed every 2 days.

383

384 **Live-image microscopy and infectious center analyses.** Image acquisition was performed
385 using an All-in-one-Fluorescence Microscope BZ-X800E (Keyence Corporation of America) with
386 a 4X objective. Images from each culture were arranged sequentially by time post-infection. A
387 blinded individual tracked individual infectious centers over the time course of the experiment
388 and determined which day post-infection the infectious center detached. These data were
389 converted to binary and were graphed as a probability of detachment.

390

391 **Titration of MeV**. MeV-infected HAE lysates for titration analysis were scraped and collected in
392 serum-free medium and 10-fold serially diluted. Serial dilutions were plated in the 96-well flat-

393 bottom plate containing Vero-hSLAM cells. 3 days post-infection, cells were titrated using
394 $TCID_{50}$/mL analysis.
395
396 **LDH cytotoxicity colormetric assay.** HAE cultures were infected and supernatants from the
397 basolateral chamber were collected. Each cultures received fresh medium after collection. LDH
398 release was detected following the manufacturer's protocol (BioVision; #K311). Briefly,
399 supernatant and reaction mixture were mixed 1:1 and incubated in a 96-well Maxi-Sorp
400 Immunoplate (Thermo Fisher Scientific; #439454). After 30 minutes at room temperature,
401 absorbance was measured at 490_{OD}. Percent cytotoxicity was measured using the following
402 formula: (test sample – low control) ÷ (high control – low control). Mock-infected supernatants
403 served as the low controls. High control samples were obtained by incubating cells with media
404 containing 0.1% Triton X-100 for 30 minutes at 37°C, followed by media collection. This method
405 allows for complete cell death, and therefore maximum LDH release, to occur.
406
407 **Sectioning HAE.** HAE were fixed with 2% paraformaldehyde for 15 minutes at room
408 temperature. Filters were excised from the transwell, submerged in Scigen Tissue-Plus O.C.T.
409 Compound (Thermo Fisher Scientific; #23-730-571), and frozen. 10 μm sections were collected
410 with a Microm Cryostat HM505E (Leica) and immunostained following the protocols listed
411 above.
412
413 **Statistics**. Statistical tests listed in the figure legends were performed in GraphPad Prism
414 version 10.1.1. Alpha values were set at 0.05. Unless otherwise indicated, numerical data are
415 presented as mean ± standard deviation (SD).
416
417 ACKNOWLEDGEMENTS
418 We thank Roberto Cattaneo for providing fluorescent MeVs and guidance. Additionally, we thank
419 Jennifer Bartlett for her thoughtful review of this manuscript. We acknowledge the support of the
420 University of Iowa Central Microscopy Research Facility, the Genomics Division of the Iowa
421 Institute of Human Genetics, and the In Vitro Models and Cell Culture Core.
422
423 FUNDING
424 This work was supported by the National Institutes of Health: NIH R01 AL-132402 and T32 AL-
425 007533.
426

427 AUTHOR CONTRIBUTIONS

428 Conceptualization: Camilla E. Hippee, Brajesh K. Singh, Patrick L. Sinn.

429 Data curation: Camilla E. Hippee.

430 Formal Analysis: Camilla E. Hippee, Lorellin A. Durnell, Justin W. Kaufman.

431 Funding Acquisition: Camilla E. Hippee, Patrick L. Sinn.

432 Investigation: Camilla E. Hippee, Lorellin A. Durnell, Justin W. Kaufman, Eileen Murray.

433 Visualization: Camilla E. Hippee, Lorellin A. Durnell, Justin W. Kaufman.

434 Writing – original draft: Camilla E. Hippee.

435 Writing – review & editing: Camilla E. Hippee, Lorellin A. Durnell, Patrick L. Sinn.

436

437 REFERENCES

438 1. Guerra FM, Bolotin S, Lim G, Heffernan J, Deeks SL, Li Y, et al. The basic reproduction
439 number (R(0)) of measles: a systematic review. Lancet Infect Dis. 2017;17(12):e420-e8.
440 2. Reis J, Shaman J. Retrospective Parameter Estimation and Forecast of Respiratory
441 Syncytial Virus in the United States. PLoS Comput Biol. 2016;12(10):e1005133.
442 3. Anderson RM, May RM. Directly transmitted infections diseases: control by vaccination.
443 Science. 1982;215(4536):1053-60.
444 4. Anderson RM, May RM. Age-related changes in the rate of disease transmission:
445 implications for the design of vaccination programmes. J Hyg (Lond). 1985;94(3):365-436.
446 5. Partnership MR. Measles Remains a Serious Threat: WHO and UNICEF National
447 Immunization Coverage Data Shows 2023 [Available from:
448 https://measlesrubellapartnership.org/measles-remains-a-serious-threat-who-and-unicef-
449 national-immunization-coverage-data-shows/.
450 6. Kaufman JW, Singh BK, Durnell LA, Sinn PL. Representative measles virus infection
451 requires appropriate airway epithelia culture conditions. J Virol. 2023:e0105123.
452 7. Karp PH, Moninger TO, Weber SP, Nesselhauf TS, Launspach JL, Zabner J, et al. An in
453 vitro model of differentiated human airway epithelia. Methods for establishing primary cultures.
454 Methods Mol Biol. 2002;188:115-37.
455 8. Pezzulo AA, Starner TD, Scheetz TE, Traver GL, Tilley AE, Harvey BG, et al. The air-
456 liquid interface and use of primary cell cultures are important to recapitulate the transcriptional
457 profile of in vivo airway epithelia. Am J Physiol Lung Cell Mol Physiol. 2011;300(1):L25-31.
458 9. Delpeut S, Noyce RS, Richardson CD. The tumor-associated marker, PVRL4 (nectin-4),
459 is the epithelial receptor for morbilliviruses. Viruses. 2014;6(6):2268-86.
460 10. Muhlebach MD, Mateo M, Sinn PL, Prufer S, Uhlig KM, Leonard VH, et al. Adherens
461 junction protein nectin-4 is the epithelial receptor for measles virus. Nature.
462 2011;480(7378):530-3.
463 11. Ferreira CS, Frenzke M, Leonard VH, Welstead GG, Richardson CD, Cattaneo R.
464 Measles virus infection of alveolar macrophages and dendritic cells precedes spread to
465 lymphatic organs in transgenic mice expressing human signaling lymphocytic activation
466 molecule (SLAM, CD150). J Virol. 2010;84(6):3033-42.
467 12. Tatsuo H, Ono N, Tanaka K, Yanagi Y. SLAM (CDw150) is a cellular receptor for measles
468 virus. Nature. 2000;406(6798):893-7.
469 13. Singh BK, Hornick AL, Krishnamurthy S, Locke AC, Mendoza CA, Mateo M, et al. The
470 Nectin-4/Afadin Protein Complex and Intercellular Membrane Pores Contribute to Rapid Spread
471 of Measles Virus in Primary Human Airway Epithelia. J Virol. 2015;89(14):7089-96.

472 14. Sinn PL, Williams G, Vongpunsawad S, Cattaneo R, McCray PB, Jr. Measles virus
473 preferentially transduces the basolateral surface of well-differentiated human airway epithelia. J
474 Virol. 2002;76(5):2403-9.
475 15. Ludlow M, de Vries RD, Lemon K, McQuaid S, Millar E, van Amerongen G, et al.
476 Infection of lymphoid tissues in the macaque upper respiratory tract contributes to the
477 emergence of transmissible measles virus. J Gen Virol. 2013;94(Pt 9):1933-44.
478 16. Ludlow M, Lemon K, de Vries RD, McQuaid S, Millar EL, van Amerongen G, et al.
479 Measles virus infection of epithelial cells in the macaque upper respiratory tract is mediated by
480 subepithelial immune cells. J Virol. 2013;87(7):4033-42.
481 17. Leser GP, Lamb RA. Influenza virus assembly and budding in raft-derived
482 microdomains: a quantitative analysis of the surface distribution of HA, NA and M2 proteins.
483 Virology. 2005;342(2):215-27.
484 18. El Najjar F, Schmitt AP, Dutch RE. Paramyxovirus glycoprotein incorporation, assembly
485 and budding: a three way dance for infectious particle production. Viruses. 2014;6(8):3019-54.
486 19. Pinto AL, Rai RK, Brown JC, Griffin P, Edgar JR, Shah A, et al. Ultrastructural insight into
487 SARS-CoV-2 entry and budding in human airway epithelium. Nat Commun. 2022;13(1):1609.
488 20. Kerr SL, Mathew C, Ghildyal R. Rhinovirus and Cell Death. Viruses. 2021;13(4).
489 21. Hippee CE, Singh BK, Thurman AL, Cooney AL, Pezzulo AA, Cattaneo R, et al. Measles
490 virus exits human airway epithelia within dislodged metabolically active infectious centers. PLoS
491 Pathog. 2021;17(8):e1009458.
492 22. Bischoff WE, McNall RJ, Blevins MW, Turner J, Lopareva EN, Rota PA, et al. Detection
493 of Measles Virus RNA in Air and Surface Specimens in a Hospital Setting. J Infect Dis.
494 2016;213(4):600-3.
495 23. Lin WW, Tsay AJ, Lalime EN, Pekosz A, Griffin DE. Primary differentiated respiratory
496 epithelial cells respond to apical measles virus infection by shedding multinucleated giant cells.
497 Proc Natl Acad Sci U S A. 2021;118(11).
498 24. Le Bras GF, Taubenslag KJ, Andl CD. The regulation of cell-cell adhesion during
499 epithelial-mesenchymal transition, motility and tumor progression. Cell Adh Migr. 2012;6(4):365-
500 73.
501 25. Shirogane Y, Takeda M, Tahara M, Ikegame S, Nakamura T, Yanagi Y. Epithelial-
502 mesenchymal transition abolishes the susceptibility of polarized epithelial cell lines to measles
503 virus. J Biol Chem. 2010;285(27):20882-90.
504 26. Kalluri R, Weinberg RA. The basics of epithelial-mesenchymal transition. J Clin Invest.
505 2009;119(6):1420-8.
506 27. Olivera A, Kohama T, Edsall L, Nava V, Cuvillier O, Poulton S, et al. Sphingosine kinase
507 expression increases intracellular sphingosine-1-phosphate and promotes cell growth and
508 survival. J Cell Biol. 1999;147(3):545-58.
509 28. Seo YJ, Blake C, Alexander S, Hahm B. Sphingosine 1-phosphate-metabolizing
510 enzymes control influenza virus propagation and viral cytopathogenicity. J Virol.
511 2010;84(16):8124-31.
512 29. Seo YJ, Pritzl CJ, Vijayan M, Bomb K, McClain ME, Alexander S, et al. Sphingosine
513 kinase 1 serves as a pro-viral factor by regulating viral RNA synthesis and nuclear export of viral
514 ribonucleoprotein complex upon influenza virus infection. PLoS One. 2013;8(8):e75005.
515 30. Vijayan M, Seo YJ, Pritzl CJ, Squires SA, Alexander S, Hahm B. Sphingosine kinase 1
516 regulates measles virus replication. Virology. 2014;450-451:55-63.
517 31. Carr JM, Mahalingam S, Bonder CS, Pitson SM. Sphingosine kinase 1 in viral infections.
518 Rev Med Virol. 2013;23(2):73-84.
519 32. Monick MM, Cameron K, Powers LS, Butler NS, McCoy D, Mallampalli RK, et al.
520 Sphingosine kinase mediates activation of extracellular signal-related kinase and Akt by
521 respiratory syncytial virus. Am J Respir Cell Mol Biol. 2004;30(6):844-52.

522 33. Gu Y, Forostyan T, Sabbadini R, Rosenblatt J. Epithelial cell extrusion requires the
523 sphingosine-1-phosphate receptor 2 pathway. J Cell Biol. 2011;193(4):667-76.
524 34. Gudipaty SA, Rosenblatt J. Epithelial cell extrusion: Pathways and pathologies. Semin
525 Cell Dev Biol. 2017;67:132-40.
526 35. Ohsawa S, Vaughen J, Igaki T. Cell Extrusion: A Stress-Responsive Force for Good or
527 Evil in Epithelial Homeostasis. Dev Cell. 2018;44(3):284-96.
528 36. Eisenhoffer GT, Loftus PD, Yoshigi M, Otsuna H, Chien CB, Morcos PA, et al. Crowding
529 induces live cell extrusion to maintain homeostatic cell numbers in epithelia. Nature.
530 2012;484(7395):546-9.
531 37. Rosenblatt J, Raff MC, Cramer LP. An epithelial cell destined for apoptosis signals its
532 neighbors to extrude it by an actin- and myosin-dependent mechanism. Curr Biol.
533 2001;11(23):1847-57.
534 38. Durnell LA, Hippee CE, Cattaneo R, Bartlett JA, Singh BK, Sinn PL. Interferon-
535 independent processes constrain measles virus cell-to-cell spread in primary human airway
536 epithelial cells. Microbiol Spectr. 2023:e0136123.
537 39. Elzamly S, Badri N, Padilla O, Dwivedi AK, Alvarado LA, Hamilton M, et al. Epithelial-
538 Mesenchymal Transition Markers in Breast Cancer and Pathological Responseafter
539 Neoadjuvant Chemotherapy. Breast Cancer (Auckl). 2018;12:1178223418788074.
540 40. Scott LE, Weinberg SH, Lemmon CA. Mechanochemical Signaling of the Extracellular
541 Matrix in Epithelial-Mesenchymal Transition. Front Cell Dev Biol. 2019;7:135.
542 41. Yang J, Antin P, Berx G, Blanpain C, Brabletz T, Bronner M, et al. Guidelines and
543 definitions for research on epithelial-mesenchymal transition. Nat Rev Mol Cell Biol.
544 2020;21(6):341-52.
545 42. Zeisberg M, Neilson EG. Biomarkers for epithelial-mesenchymal transitions. J Clin
546 Invest. 2009;119(6):1429-37.
547 43. Halder SK, Beauchamp RD, Datta PK. A specific inhibitor of TGF-beta receptor kinase,
548 SB-431542, as a potent antitumor agent for human cancers. Neoplasia. 2005;7(5):509-21.
549 44. Hao Y, Baker D, Ten Dijke P. TGF-beta-Mediated Epithelial-Mesenchymal Transition and
550 Cancer Metastasis. Int J Mol Sci. 2019;20(11).
551 45. Wee K, Hediyeh-Zadeh S, Duszyc K, Verma S, B NN, Khare S, et al. Snail induces
552 epithelial cell extrusion by regulating RhoA contractile signalling and cell-matrix adhesion. J Cell
553 Sci. 2020;133(13).
554 46. Hargest V, Bub T, Neale G, Schultz-Cherry S. Astrovirus-induced epithelial-
555 mesenchymal transition via activated TGF-beta increases viral replication. PLoS Pathog.
556 2022;18(4):e1009716.
557 47. Zhang Z, Zou J, Shi Z, Zhang B, Etienne-Mesmin L, Wang Y, et al. IL-22-induced cell
558 extrusion and IL-18-induced cell death prevent and cure rotavirus infection. Sci Immunol.
559 2020;5(52).
560 48. Moshiri J, Craven AR, Mixon SB, Amieva MR, Kirkegaard K. Mechanosensitive extrusion
561 of Enterovirus A71-infected cells from colonic organoids. Nat Microbiol. 2023;8(4):629-39.
562 49. Eisenhoffer GT, Rosenblatt J. Bringing balance by force: live cell extrusion controls
563 epithelial cell numbers. Trends Cell Biol. 2013;23(4):185-92.
564 50. Tada M. The morphogenetic changes that lead to cell extrusion in development and cell
565 competition. Dev Biol. 2021;477:1-10.
566 51. Franco JJ, Atieh Y, Bryan CD, Kwan KM, Eisenhoffer GT. Cellular crowding influences
567 extrusion and proliferation to facilitate epithelial tissue repair. Mol Biol Cell. 2019;30(16):1890-9.
568 52. Katoh H, Fujita Y. Epithelial homeostasis: elimination by live cell extrusion. Curr Biol.
569 2012;22(11):R453-5.
570 53. Kuipers D, Mehonic A, Kajita M, Peter L, Fujita Y, Duke T, et al. Epithelial repair is a two-
571 stage process driven first by dying cells and then by their neighbours. J Cell Sci. 2014;127(Pt
572 6):1229-41.

573 54. Song L, Xiong H, Li J, Liao W, Wang L, Wu J, et al. Sphingosine kinase-1 enhances
574 resistance to apoptosis through activation of PI3K/Akt/NF-kappaB pathway in human non-small
575 cell lung cancer. Clin Cancer Res. 2011;17(7):1839-49.
576 55. Kim KK, Kugler MC, Wolters PJ, Robillard L, Galvez MG, Brumwell AN, et al. Alveolar
577 epithelial cell mesenchymal transition develops in vivo during pulmonary fibrosis and is
578 regulated by the extracellular matrix. Proc Natl Acad Sci U S A. 2006;103(35):13180-5.
579 56. Liu H, Ma Y, He HW, Zhao WL, Shao RG. SPHK1 (sphingosine kinase 1) induces
580 epithelial-mesenchymal transition by promoting the autophagy-linked lysosomal degradation of
581 CDH1/E-cadherin in hepatoma cells. Autophagy. 2017;13(5):900-13.
582 57. Liu SQ, Xu CY, Wu WH, Fu ZH, He SW, Qin MB, et al. Sphingosine kinase 1 promotes
583 the metastasis of colorectal cancer by inducing the epithelial-mesenchymal transition mediated
584 by the FAK/AKT/MMPs axis. Int J Oncol. 2019;54(1):41-52.
585 58. He F, Fan M, Jin Y, Wang H, Ding L, Fan J, et al. Sphingosine kinase 1 inhibition
586 decreases the epithelial-mesenchymal transition and ameliorates renal fibrosis via modulating
587 NF-kappaB signaling. Am J Transl Res. 2019;11(9):5879-87.
588 59. Riemma MA, Cerqua I, Romano B, Irollo E, Bertolino A, Camerlingo R, et al.
589 Sphingosine-1-phosphate/TGF-beta axis drives epithelial mesenchymal transition in asthma-like
590 disease. Br J Pharmacol. 2022;179(8):1753-68.
591 60. Wang W, Hind T, Lam BWS, Herr DR. Sphingosine 1-phosphate signaling induces
592 SNAI2 expression to promote cell invasion in breast cancer cells. FASEB J. 2019;33(6):7180-
593 91.
594 61. Aloia AL, Calvert JK, Clarke JN, Davies LT, Helbig KJ, Pitson SM, et al. Investigation of
595 sphingosine kinase 1 in interferon responses during dengue virus infection. Clin Transl
596 Immunology. 2017;6(7):e151.
597 62. Stewart CM, Bo Y, Fu K, Chan M, Kozak R, Apperley KY, et al. Sphingosine Kinases
598 Promote Ebola Virus Infection and Can Be Targeted to Inhibit Filoviruses, Coronaviruses, and
599 Arenaviruses Using Late Endocytic Trafficking to Enter Cells. ACS Infect Dis. 2023;9(5):1064-
600 77.
601 63. Bonica J, Clarke CJ, Obeid LM, Luberto C, Hannun YA. Upregulation of sphingosine
602 kinase 1 in response to doxorubicin generates an angiogenic response via stabilization of Snail.
603 FASEB J. 2023;37(3):e22787.
604 64. Bonica J, Mao C, Obeid LM, Hannun YA. Transcriptional Regulation of Sphingosine
605 Kinase 1. Cells. 2020;9(11).
606 65. Cannavo A, Liccardo D, Komici K, Corbi G, de Lucia C, Femminella GD, et al.
607 Sphingosine Kinases and Sphingosine 1-Phosphate Receptors: Signaling and Actions in the
608 Cardiovascular System. Front Pharmacol. 2017;8:556.
609 66. Maceyka M, Harikumar KB, Milstien S, Spiegel S. Sphingosine-1-phosphate signaling
610 and its role in disease. Trends Cell Biol. 2012;22(1):50-60.
611 67. Rutherford C, Childs S, Ohotski J, McGlynn L, Riddick M, MacFarlane S, et al.
612 Regulation of cell survival by sphingosine-1-phosphate receptor S1P1 via reciprocal ERK-
613 dependent suppression of Bim and PI-3-kinase/protein kinase C-mediated upregulation of Mcl-
614 1. Cell Death Dis. 2013;4(11):e927.
615 68. Machesky NJ, Zhang G, Raghavan B, Zimmerman P, Kelly SL, Merrill AH, Jr., et al.
616 Human cytomegalovirus regulates bioactive sphingolipids. J Biol Chem. 2008;283(38):26148-
617 60.
618 69. Adada MM, Orr-Gandy KA, Snider AJ, Canals D, Hannun YA, Obeid LM, et al.
619 Sphingosine kinase 1 regulates tumor necrosis factor-mediated RANTES induction through p38
620 mitogen-activated protein kinase but independently of nuclear factor kappaB activation. J Biol
621 Chem. 2013;288(38):27667-79.

622 70. Alvarez SE, Harikumar KB, Hait NC, Allegood J, Strub GM, Kim EY, et al. Sphingosine-
623 1-phosphate is a missing cofactor for the E3 ubiquitin ligase TRAF2. Nature.
624 2010;465(7301):1084-8.
625 71. Xia P, Wang L, Moretti PA, Albanese N, Chai F, Pitson SM, et al. Sphingosine kinase
626 interacts with TRAF2 and dissects tumor necrosis factor-alpha signaling. J Biol Chem.
627 2002;277(10):7996-8003.
628 72. Milara J, Navarro R, Juan G, Peiro T, Serrano A, Ramon M, et al. Sphingosine-1-
629 phosphate is increased in patients with idiopathic pulmonary fibrosis and mediates epithelial to
630 mesenchymal transition. Thorax. 2012;67(2):147-56.
631 73. Sukocheva OA, Hu DG, Meech R, Bishayee A. Divergence of Intracellular Trafficking of
632 Sphingosine Kinase 1 and Sphingosine-1-Phosphate Receptor 3 in MCF-7 Breast Cancer Cells
633 and MCF-7-Derived Stem Cell-Enriched Mammospheres. Int J Mol Sci. 2021;22(9).
634 74. Hait NC, Allegood J, Maceyka M, Strub GM, Harikumar KB, Singh SK, et al. Regulation
635 of histone acetylation in the nucleus by sphingosine-1-phosphate. Science.
636 2009;325(5945):1254-7.
637 75. Chugh P, Clark AG, Smith MB, Cassani DAD, Dierkes K, Ragab A, et al. Actin cortex
638 architecture regulates cell surface tension. Nat Cell Biol. 2017;19(6):689-97.
639 76. Kurosaka S, Kashina A. Cell biology of embryonic migration. Birth Defects Res C
640 Embryo Today. 2008;84(2):102-22.
641 77. Eden E, Lipson D, Yogev S, Yakhini Z. Discovering motifs in ranked lists of DNA
642 sequences. PLoS Comput Biol. 2007;3(3):e39.
643 78. Eden E, Navon R, Steinfeld I, Lipson D, Yakhini Z. GOrilla: a tool for discovery and
644 visualization of enriched GO terms in ranked gene lists. BMC Bioinformatics. 2009;10:48.
645 79. Leonard VH, Sinn PL, Hodge G, Miest T, Devaux P, Oezguen N, et al. Measles virus
646 blind to its epithelial cell receptor remains virulent in rhesus monkeys but cannot cross the
647 airway epithelium and is not shed. J Clin Invest. 2008;118(7):2448-58.
648 80. Ono N, Tatsuo H, Hidaka Y, Aoki T, Minagawa H, Yanagi Y. Measles viruses on throat
649 swabs from measles patients use signaling lymphocytic activation molecule (CDw150) but not
650 CD46 as a cellular receptor. J Virol. 2001;75(9):4399-401.
651

652 FIGURE LEGENDS

653 **Fig 1. Single-cell RNA sequencing implicates two detachment pathways.** (A) Schematic
654 depiction of infectious center formation and detachment. Green cells represent MeV-infected
655 cells. Cell-to-cell spread of MeV over 3-5 days results in an infectious center, left. Beginning
656 around 5 days post-infection, infectious centers begin to detach as a unit from the rest of the
657 epithelial layer, right. (B) Differentially expressed gene lists of MeV-infected HAE were derived
658 from a previously published scRNA-seq dataset (21). Genes with increased mRNA levels in
659 MeV-infected HAE at 3 days post-infection vs. mock-infected HAE were analyzed with biological
660 process gene ontology. Related gene ontology terms are connected with arrows. (C) Heatmap
661 of mRNA expression for EMT-related genes in MeV-infected HAE at day 3 post-infection. Gene
662 expression was normalized to mock-infected HAE and derived from the scRNA-seq dataset. (D)
663 Cells from the scRNA-seq dataset are visualized via t-SNE plot. Cells are clustered by similar
664 gene transcription. Cell types were assigned to clusters using cell type markers described in
665 (21). (E) Cells expressing SNAI2, a transcriptional regulator of EMT, are colored according to

666 mRNA expression. A cluster of cells with high SNAI2 expression is highlighted in the inset. (F)
667 SK1, which promotes LCE, is also expressed in this cell cluster (see inset).
668
669 **Fig 2. EMT is activated within infectious centers.** HAE infected with MeV-mCherry were fixed
670 at 3- and 7-days post-infection. Cultures were immunostained for βCAT (A), ZO-1 (B), or ECAD
671 (C). Confocal images of 3 infectious centers were collected per donor (n=3). Representative
672 images are shown. Corresponding z-stacks are shown below each image. Blue = DAPI. (D)
673 Percent cytoskeleton breakdown was calculated by dividing total area of breakdown for each
674 cytoskeletal protein by the total area of the infectious center. Multiple t-tests were performed. *
675 $p<0.05$.
676
677 **Fig 3. EMT contributes to infectious center detachment.** (A) Graphic representation of
678 infectious center detachment assay. Images are taken each day post-infection. Individual
679 infectious centers (green dot) are tracked until they detach (represented by a red X). The day
680 post-infection at which each infectious center detaches is recorded. (B) HAE were treated with
681 either SB431542 (SB) or a vehicle control (DMSO) for 24 hours before being infected at an MOI
682 of 1 (MeV-GFP). Data from the detachment assay are graphed as a probability of detachment
683 (i.e., percent of infectious centers detached at each time point). A Gehan-Breslow-Wilcoxon test
684 was performed and indicated that there was a statistical significance between the two curves. *
685 $p<0.05$. (C) Whole culture lysates, which may include detached infectious centers in the apical
686 space, were collected from MeV-infected HAE (with either SB treatment or vehicle) at the
687 indicated timepoint for titration via $TCID_{50}$. A one-way ANOVA with multiple comparisons was
688 performed. ns = not significant. (D) Live fluorescent images were collected at 3 days post-
689 infection. Numbers and size (E) of infectious centers were measured with ImageJ. Counts were
690 normalized to vehicle controls and displayed as a percentage. Shapes indicate individual donors
691 (n=5). Student's t-test. (E) Dots indicate individual infectious centers. Median ± interquartile
692 range. Student's t-test. (F) Cytotoxicity of SB treatment was determined via LDH assay at 3
693 days post-infection with MeV. SB and DMSO treated cells had comparable cytotoxicity when
694 normalized to Triton X-100 treated cells (+ control). One-way ANOVA.
695
696 **Fig 4. LCE is activated within infectious centers.** (A) Diagram of SK1's function. SK1
697 phosphorylates sphingosine to make S1P. (B) Heatmap of LCE-related gene expression in ISG-
698 high cells at 3 days post-infection. Shade of red indicates increased fold change over mock-
699 infected cells. (C) *En face* immunostaining of SK1 in HAE infected with MeV-mCherry at 3 days

post-infection. Scale bar = 50 μm. (D) Immunostained sections of MeV-mCherry infected HAE at 3 days post-infection. Arrows indicate cells with SK1 staining localized to the nucleus. Scale bar = 25 μm.

Fig 5. LCE contributes to infectious center detachment. (A) An SK1 inhibitor (SKI-II) or (C) exogenous S1P was applied 1-day post-infection with MeV. The infectious center detachment assay was performed as described in **Fig 3**. Gehan-Breslow-Wilcoxon tests were performed and indicated that there were statistical significances between the curves. * $p<0.05$; **** $p<0.0001$. (B) Cell lysates were collected from MeV-infected HAE treated with SKI-II or (D) S1P at the indicated timepoint for titration via $TCID_{50}$. A one-way ANOVA with multiple comparisons was performed. ns = not significant.

Fig S1. Characterization of ISG-high cells. (A) The t-SNE plot from Fig 1 with GFP status overlayed. GFP+ indicates infected cells, GFP- indicates uninfected cells from MeV-infected HAE. Mock indicates cells mock infected. The box highlights the ISG-high cell cluster. The adjoining graph identifies the division of ISG-high cells that are GFP+ or GFP-. (B) Violin plot of SNAI2 expression across cell clusters. (C) Violin plot of SK1 expression across cell clusters.

Fig S2. qRT-PCR confirmation of scRNA-seq. (A) scRNA-seq results were confirmed with qRT-PCR. Transcript changes of MeV-infected HAE are shown as a fold change over mock-infected cells. One-way ANOVA was performed. * $p<0.05$, ** $p<0.01$. (B) Apical (open shapes) and basolateral (filled shapes) secretions were collected from mock- and MeV-infected HAE at 3 days post-infection. Protein content was measured using a TGF-β ELISA kit. Shapes indicate distinct donors (n=3). Paired Student's t-test; * $p<0.05$. (C) HAE infected with MeV-mCherry were fixed at 7 days post-infection and immunostained for ezrin. A z-stack image is shown below. The arrow points to ezrin staining that has been disturbed within the infectious center. Blue = DAPI. Scale bar = 50 μm.

Fig S3. Impact of LCE treatments on infection kinetics. Live fluorescent images of (A-B) SKI-II treated or (C-D) S1P treated HAE were collected at 3 days post-infection with MeV. Numbers (A and C) and size (B and D) of infectious centers were measured with ImageJ. Counts were normalized to vehicle controls and displayed as a percentage. Shapes indicate individual donors (n=4 in A; n=5 in C). Student's t-test; ns = not significant. (B and D) Dots indicate individual infectious centers. Median ± interquartile range. Student's t-test. (E)

734 Cytotoxicity of SB treatment was determined via LDH assay at 3 days post-infection with MeV.
735 SKI-II, S1P, and DMSO treated cells had comparable cytotoxicity when normalized to Triton X-
736 100 treated cells (+ control). One-way ANOVA.
737
738 **S1 Table. Primer sequences for qRT-PCR analysis.**

Gene name	Direction	Sequence
MMP1	Forward	CCTAGTCTATTCATAGCTAATCAAGAGGATGT
	Reverse	AGTGGAGGAAAGCTGTGCATAC
MMP10	Forward	ATCTGAGATGCCAGCCAAGT
	Reverse	AGGGTTCCAGTGGGATCTTC
TGFB1	Forward	GGCCTCCCCACCACACCAG
	Reverse	GCCGCAGCTTGGACAGGATC
SNAI2	Forward	ATCTGCGGCAAGGCGTTTTCCA
	Reverse	GAGCCCTCAGATTTGACCTGTC
SMAD3	Forward	GCCTGTGCTGGAACATCATC
	Reverse	TTGCCCTCATGTGTGCTCTT
SFRS9	Forward	TGCGTAAACTGGATGACACC
	Reverse	CCTGCTTTGGTATGGAGAGTC

739

Fig 1. Single-cell RNA sequencing implicates two detachment pathways.

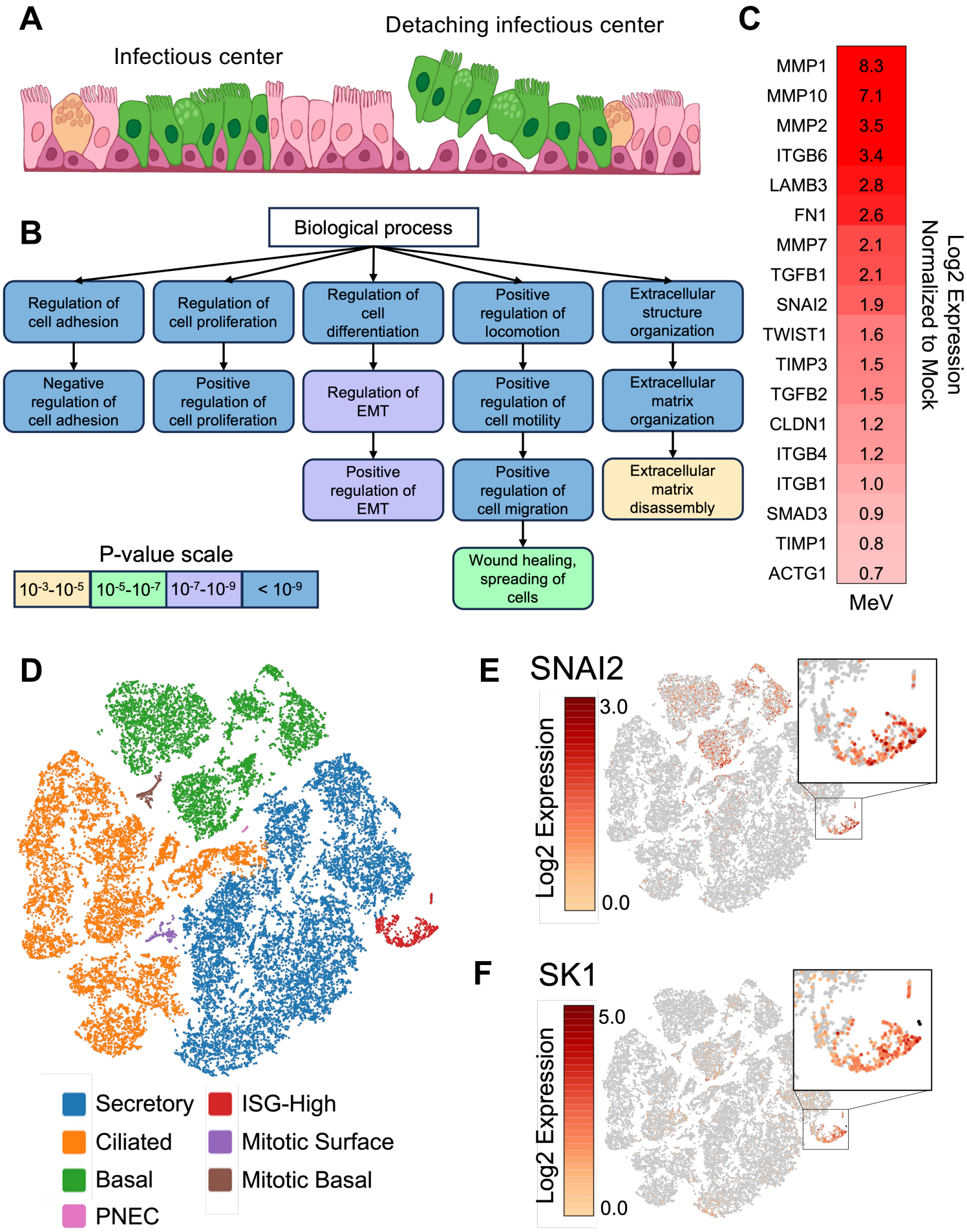

Fig 2. EMT is activated within infectious centers.

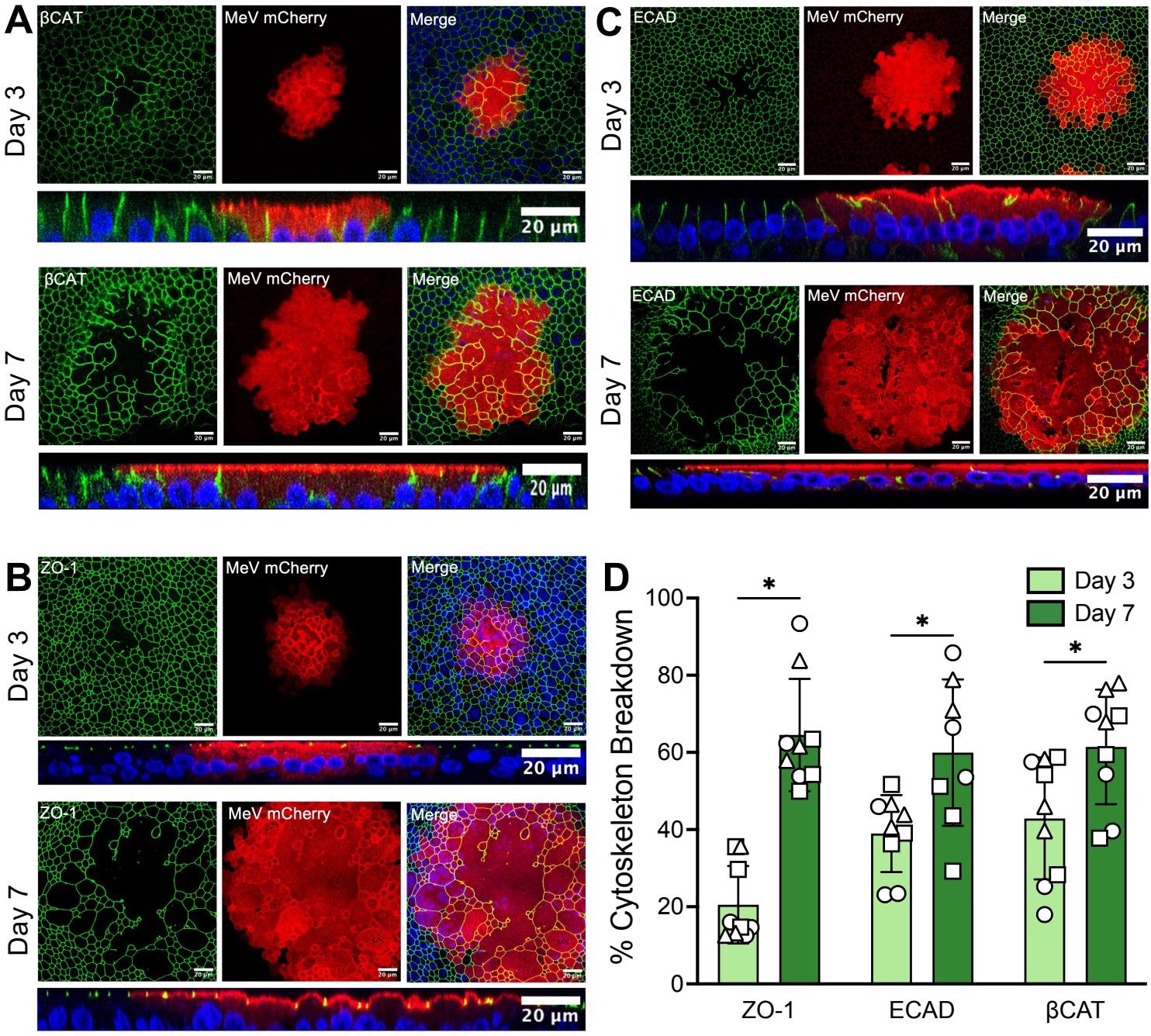

Fig 3. EMT contributes to infectious center detachment.

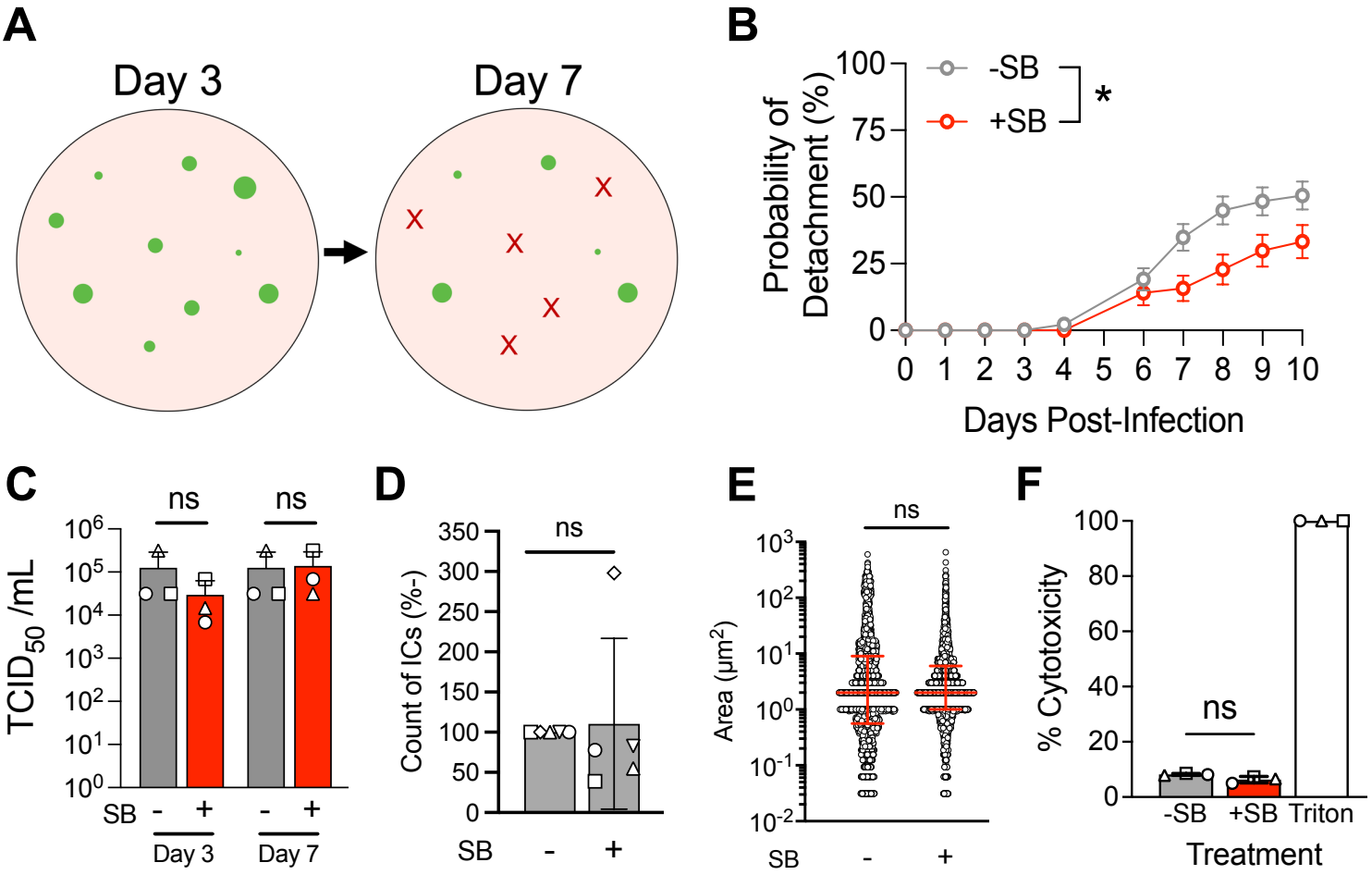

Fig 4. LCE is activated within infectious centers.

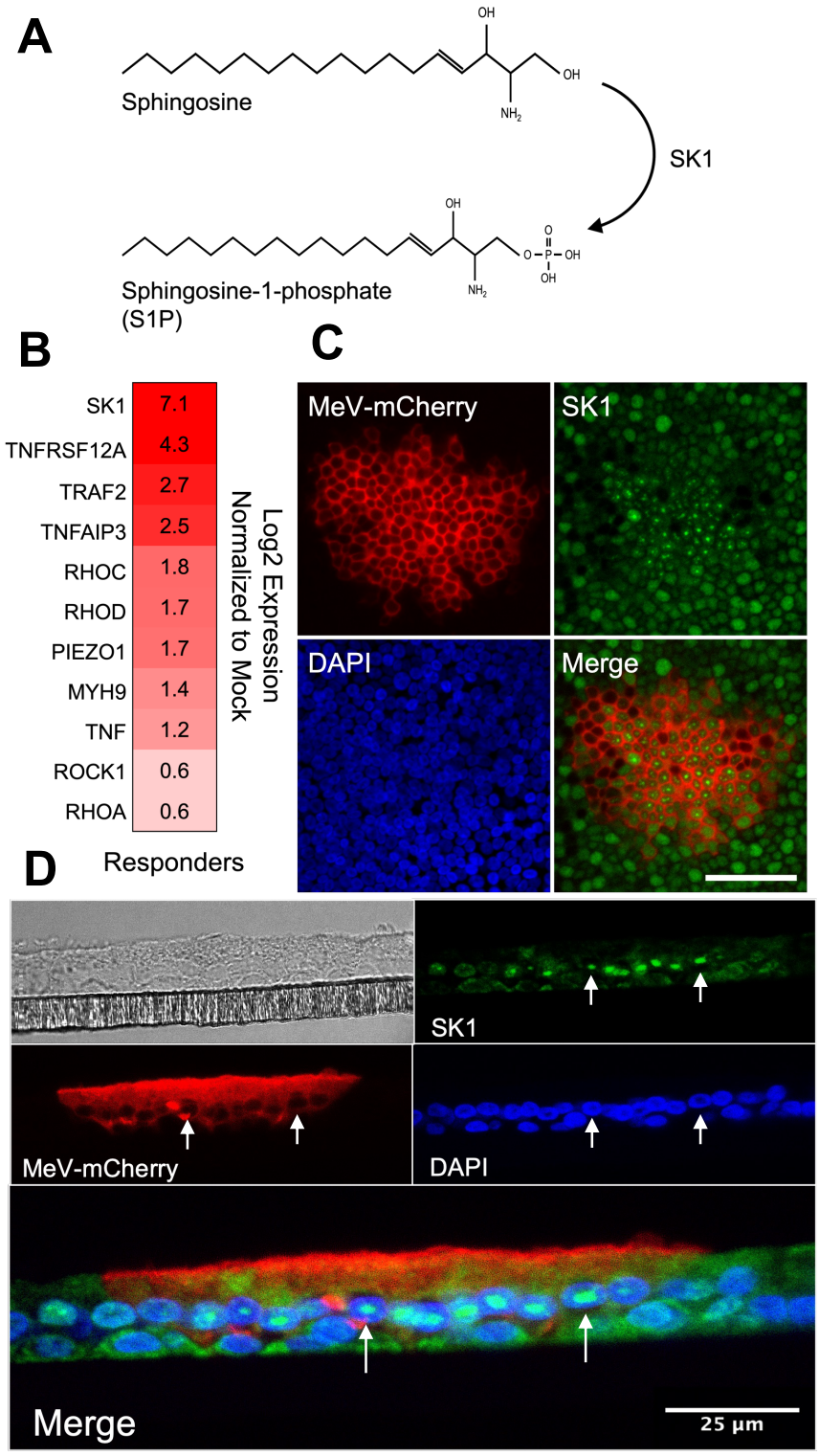
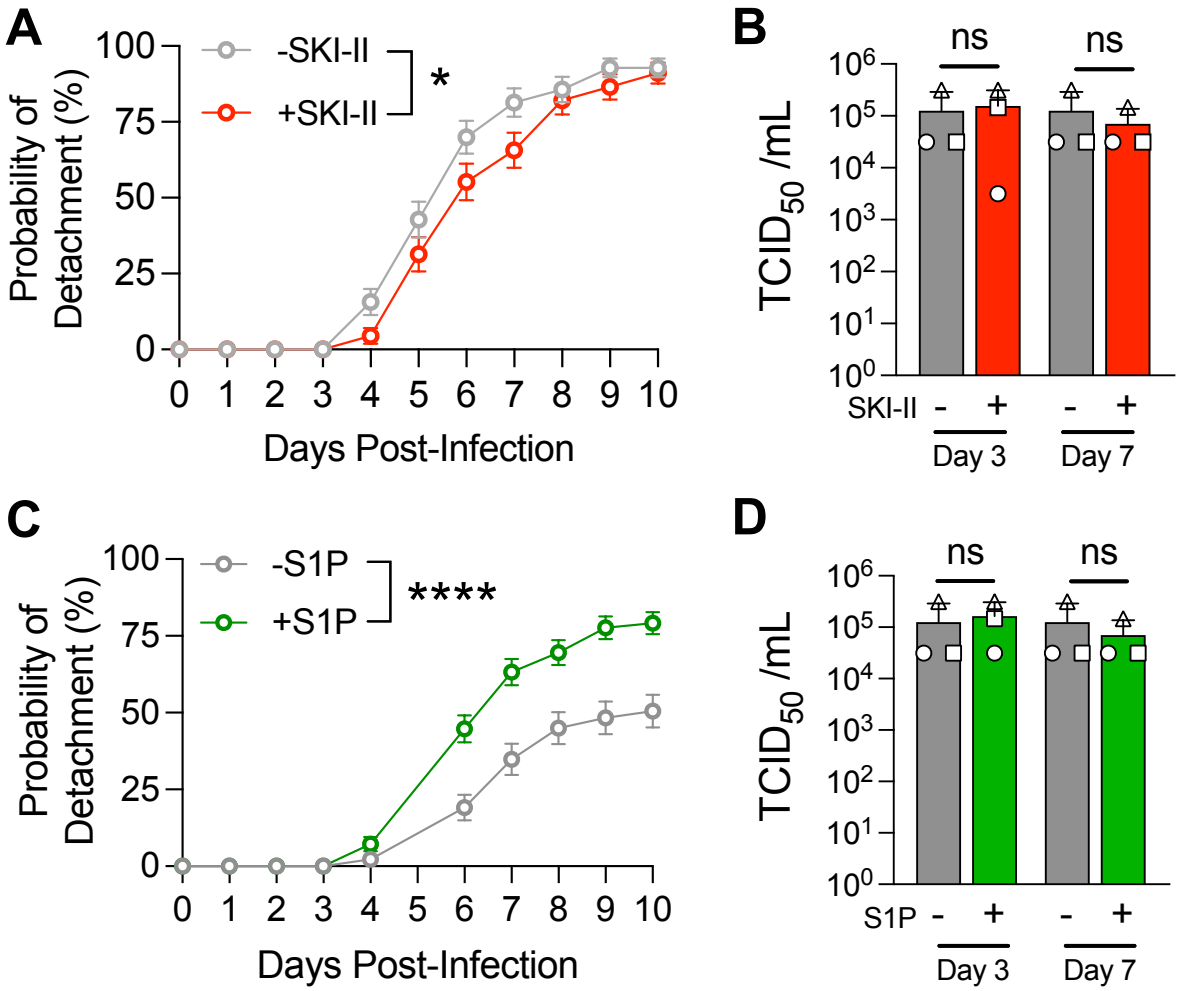
Fig 5. LCE contributes to infectious center detachment.